Nanoscale

Accepted Manuscript

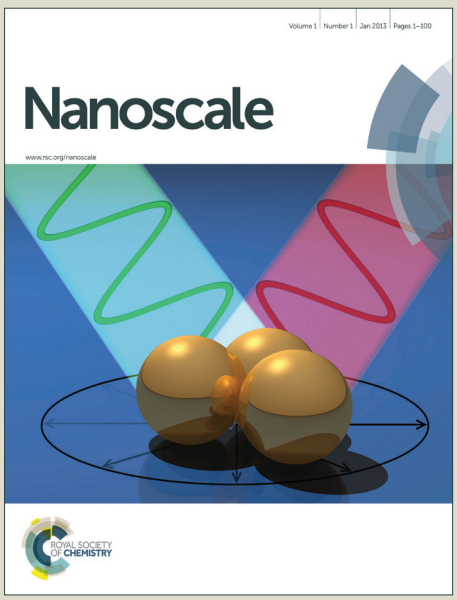

ROYAL SOCIETY OF CHEMISTRY

www.rsc.org/nanoscale

Journal Name

RSCPublishing

ARTICLE

Graphene as an Atomically Thin Barrier to Cu Diffusion into Si

Cite this: DOI: 10.1039/xoxxooooox

Juree Hong[a], Sanggeun Lee[a], Seulah Lee[a], Heetak Han[a], Chandreswar Mahata[a], Han-Wool Yeon[b], Bonwoong Koo[c], Seong-Il Kim[c], Taewook Nam[d], Byung-Wook Min[e], Young-Woon Kim[c], Hyungjun Kim[d], Young-Chang Joo[b], and Taeyoon Lee*[a]

Received ooth [month] [year],
Accepted ooth [month] [year]

DOI: 10.1039/xoxxooooox

www.rsc.org/

The evolution of copper-based interconnects requires the realization of an ultrathin diffusion barrier layer between Cu interconnect and insulating layers. The present work reports the use of atomically thin layer graphene as a diffusion barrier for Cu metallization. The diffusion barrier performance is investigated by varying grain size and thickness of graphene layer; single-layer graphene of average grain size 2±1 μm (denoted small-grain SLG), single-layer graphene of average grain size 10±2 μm (denoted large-grain SLG), and multi-layer graphene (MLG) of thickness 5–10 nm. The thermal stability of these barriers is investigated after annealing Cu/small-grain SLG/Si, Cu/large-grain SLG/Si, and Cu/MLG/Si stacks at different temperatures ranging from 500 to 900 °C. X-ray diffraction, transmission electron microscopy, and time-of-flight secondary ion mass spectroscopy analyses confirm that the small-grain SLG barrier is stable after annealing up to 700 °C and that the large-grain SLG and MLG barriers are stable after annealing at 900 °C for 30 min under a mixed Ar and H_2 gas atmosphere. The time-dependent dielectric breakdown (TDDB) test is used to evaluate graphene as a Cu diffusion barrier under real device operating conditions, revealing that both large-grain SLG and MLG have excellent barrier performance, while small-grain SLG fails quickly. Notably, the large-grain SLG acts as a better diffusion barrier than the thicker MLG in the TDDB test, indicating that the grain boundary density of a graphene diffusion barrier is more important than its thickness. The near-zero-thickness SLG is a promising Cu diffusion barrier for advanced metallization.

1. Introduction

The use of Cu interconnects in back-end-of-line (BEOL) processes has led to significant improvements over Al interconnects in Si integrated circuit technologies; namely, Cu interconnects offer lower electrical resistivity and superior electromigration resistance.[1] However, Cu atoms diffuse well into Si, forming resistive Cu-Si compounds that lead to rapid device failure[2]; thus, the use of diffusion barriers is essential for Cu interconnects. Although binary layers of Ta/TaN are considered adequate barriers due to their low solubility in Cu and their high thermal stability, [3] critical challenges have emerged with the continuous scaling down of feature size. The International Technology Roadmap for Semiconductors recently reported that interconnects with a line-width of 22 nm require a diffusion barrier less than 2 nm thick.[4] However, thinning down the thickness of diffusion barriers to this scale considerably increases their effective resistivities by increasing the relative area of grain boundaries and the effect of interface scattering.[5,6] Besides, the deposition of ultrathin diffusion barriers with excellent barrier continuity and uniformity has always been a challenging task.[5,7]

Much effort has been devoted to the development of an alternate Cu diffusion barrier material besides Ta/TaN layers, to ensure low resistivity while obtaining good conformality with the requirement of sub-22-nm interconnect technology. Koike *et al*. used a self-forming diffusion barrier layer of a thin CuMn alloy to reduce barrier thickness.[8] CuMn alloy thin films were deposited on SiO_2 substrates, followed by annealing to form a Mn oxide layer at the interface. Although a relatively thin barrier layer of 3–4 nm could thus be formed, the presence of the Mn oxide induce the reduction of the total BEOL conductivity, which is not desirable. Hsu *et al*. recently reported the use of 5-nm-thick RuMo alloy film as a seedless Cu diffusion barrier. This film remained stable after annealing at 700 °C and prevented interdiffusion between the Cu and Si.[9] However, successful Cu diffusion barriers that are less than 2 nm thick have not been previously reported.

Graphene, a one-atom-thick layer of carbon atoms arranged in a two-dimensional hexagonal lattice, is an excellent candidate for a Cu diffusion barrier because of its outstanding electrical and mechanical properties, thermal stability, and chemical stability.[10] Moreover, graphene is known to be impermeable to atoms, molecules, ions, fluids, and standard gases including helium.[11] Nonetheless, very few researchers have evaluated whether graphene can act as a barrier to the diffusion of metals. Kim *et al*. recently reported that graphene can effectively block the interdiffusion of Al atoms into underlying Si at temperatures up to 700 °C.[12] Kang *et al.*

studied the benefits of MLG capping on Cu interconnects for suppressing Cu electromigration.[13] However, no prior study has examined whether graphene layers can act as Cu diffusion barriers.

In this report, we systematically investigated the ability of both single-layer and multilayer graphene grown by chemical vapor deposition (CVD) to act as Cu diffusion barriers. Despite its high-temperature growth conditions, the CVD method is believed to be the most promising approach among all the techniques to produce graphene as it is inexpensive and easy for large-area production with moderate quality. Even though low-temperature CVD growth of graphene has been reported which meets the requirements for current generation CMOS technology,[14] the graphene fabricated by such methods show higher intensity of D band compared to that of high-temperature grown graphene in Raman spectrum. Thereby, we used a high-temperature growth process for the fabrication of SLG and MLG with low defects in the graphene lattice for use as diffusion barriers. Herein, we evaluated the Cu barrier performance of single-layer graphene (SLG) of 2 μm average grain size (denoted small-grain SLG), SLG of 10 μm average grain size (denoted large-grain SLG), and multilayer graphene (MLG) of 5–10 nm thickness by annealing in a vacuum chamber for 30 min at temperatures ranging from 500 to 900 °C. X-ray diffraction (XRD), transmission electron microscopy (TEM) analyses, and the time-of-flight secondary ion mass spectroscopy (ToF-SIMS) depth profile analyses confirmed that the formation of copper silicide was effectively suppressed, even at 900 °C, by both large-grain SLG and MLG barriers. To investigate the effects of electric field and thermal stress on the diffusion barriers, we conducted time-dependent dielectric breakdown (TDDB) tests using a metal-insulator-semiconductor (MIS) structure. The barrier performance of both large-grain SLG and MLG was superior to that of thin film-grown barriers. We also found that the large-grain SLG and MLG had different blocking performance, which we attributed to their different grain sizes based on confocal Raman mapping results, optical microscope images, and field emission scanning electron microscope (FE-SEM) images.

2. Results and discussion

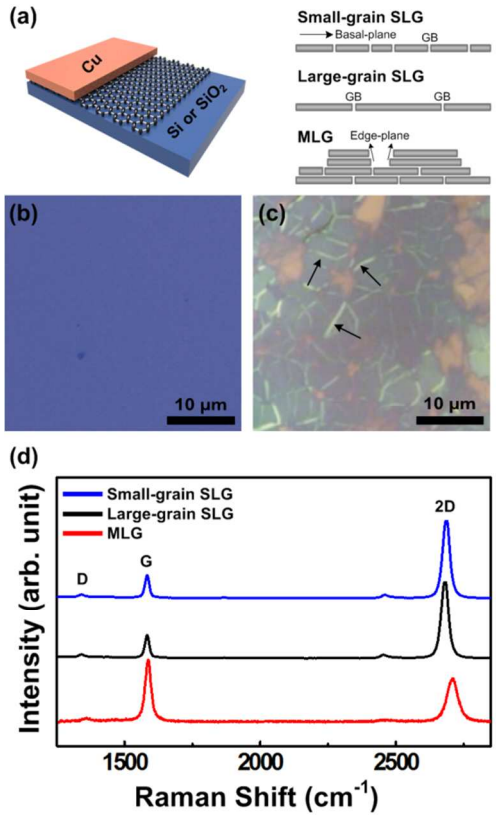

Figure 1. (a) Schematics of Cu/graphene barrier/Si or SiO_2 substrate structures. Presented graphene barriers are small-grain SLG barrier, large-grain SLG barrier, and MLG barrier. (b–c) Optical micrographs of (b) large-grain SLG and (c) MLG transferred to 300-nm-thick SiO_2/Si; black arrows indicate wrinkles on the MLG. (d) Micro-Raman spectra of small-grain SLG (blue solid line), large-grain SLG (black solid line), and MLG (red solid line).

Figure 1a shows schematics of the samples used in our experiments. In our study, we separately prepared Cu-grown SLG samples and Ni-grown MLG samples. For the Cu-grown SLG, we prepared two sets of samples: a SLG sample of grain size 1–3 μm, and a SLG sample of grain size 6–12 μm. We refer to these samples respectively as small-grain SLG and large-grain SLG. The grain size of the Ni-grown MLG was 4–6 μm. The verification of these grain sizes will be discussed in detail below. SLG samples were dominated by graphene basal planes and MLG samples were dominated by edge planes, respectively. The large-grain SLG transferred onto the SiO_2/Si substrate was nearly flat and flawless, with uniform color contrast (Figure 1b); the transferred small-grain SLG on the SiO_2/Si substrate also showed uniform color contrast (data not shown). An atomic force microscopy (AFM) measurement for a large-grain SLG/SiO_2/Si sample further confirmed the inevitable wrinkles and negligible PMMA residue (Figure S2). Contrastingly, the MLG transferred onto the SiO_2/Si substrate consisted of multilayered grains and single to multiple layers that could be identified optically by their irregularities in color, as shown in Figure 1c. In addition, the transferred MLG was rippled (see black arrows in Figure 1c), which we attributed not to the transfer process but rather to the cooling process, because graphene and Ni have considerably different thermal expansion coefficients.[15] No significant cracks or holes were evident in the SLG or MLG transferred to the SiO_2/Si substrate. Micro-Raman spectra taken from each transferred sample to verify the existence of graphene layers and the quality of the layers are shown in Figure 1d. Pristine

graphene has sharp G (~1580 cm^{-1}) and 2D (~2700 cm^{-1}) bands, with an I_G/I_{2D} intensity ratio smaller than 0.5; the 2D peak has a narrow full width at half maximum (FWHM) of 30 cm^{-1}.[16] A sharp G peak at 1583 cm^{-1} and an intense 2D peak at 2687 cm^{-1} were observed for both small- and large-grain SLG samples transferred onto SiO_2/Si. We attributed slight shifts in the 2D peaks for both small- and large-grain SLG samples to hole doping in the graphene sheets, formed by means of exposure to oxygen and moisture.[17] The FWHM of the 2D peak was approximately 35 cm^{-1}, while the I_G/I_{2D} ratio of the SLG sample was ~0.42 for both small- and large-grain SLG samples; these results indicated that the CVD-grown SLG was single-layer. The Raman spectrum of multilayered pristine graphene is characterized by an I_G/I_{2D} intensity ratio larger than 1 and by broad 2D bands.[18] The I_G/I_{2D} ratio of the transferred MLG on SiO_2/Si was 1.45, and the 2D peak had a FWHM of ~50 cm^{-1}, indicating that the transfer of the MLG onto the SiO_2 substrate was successful. A minor D peak was observed near 1350 cm^{-1} in the Raman spectra of small-grain SLG, large-grain SLG, and MLG; we attributed this peak to the formation of defects and wrinkles.[19]

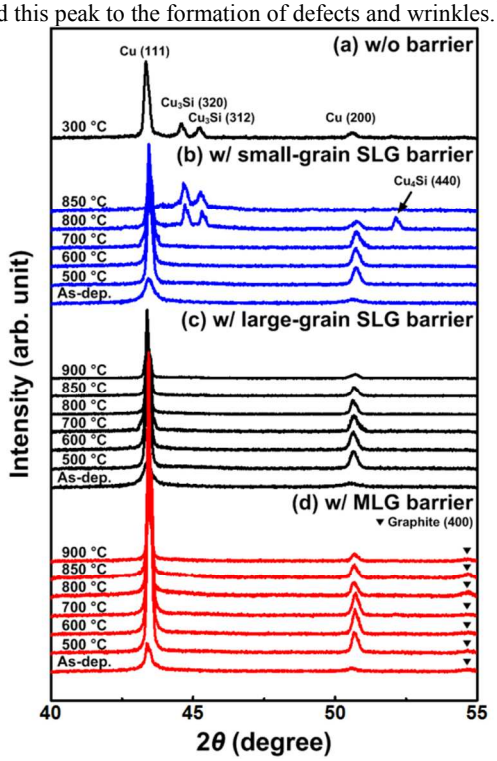

Figure 2. X-ray diffraction ω-2θ scans of (a) a Cu/Si sample after annealing at 300 °C; (b) the as-deposited Cu/small-grain SLG/Si sample and Cu/small-grain SLG/Si sample annealed at 500, 600, 700, 800, and 850 °C; (c) the as-deposited Cu/large-grain SLG/Si sample and Cu/large-grain SLG/Si sample annealed at 500, 600, 700, 800, 850, and 900 °C; (d) as-deposited Cu/MLG/Si sample and Cu/MLG/Si sample annealed at 500, 600, 700, 800, 850, and 900 °C. All annealed samples used here were annealed for 30 min; Cu/Si and the graphene-containing samples were annealed in a mixture of Ar and H_2.

To investigate the thermal stability of graphene as a diffusion barrier to Cu, we prepared and annealed at different temperatures three stacked structures: Cu/small-grain SLG/Si, Cu/large-grain SLG/Si, and Cu/MLG/Si. As a control, we also prepared a Cu/Si structure with no diffusion barrier. XRD ω-2θ scans of the Cu/Si sample after annealing at 300 °C for 30 min are shown in Figure 2a. H_2 and Ar gases were flowed into the chamber to prevent oxidation of the Cu films.[20] Noticeable diffraction peaks were detected at 43.40°, 44.61°, 45.25°, and 50.48°, corresponding to Cu(111), Cu_3Si(320), Cu_3Si(312), and Cu(200), respectively.[21] This result is coincident with the fact that copper silicides form at approximately 300 °C without barriers.[22] XRD ω-2θ scans of Cu/small-grain SLG/Si samples before and after annealing for 30 min at different temperatures ranging from 500 to 850 °C are shown in Figure 2b. In the as-deposited Cu/ small-grain SLG/Si sample, two peaks were observed at 43.40° and 50.48°, corresponding to Cu (111) and Cu (200), respectively. The higher intensity of the Cu (111) peak indicated that the preferential crystal orientation of the deposited Cu film was <111>; this orientation has higher Cu electromigration resistance than other orientations.[20,23] After annealing of the as-deposited Cu/small-grain SLG/Si sample at 500 °C, the broad peaks of the as-deposited Cu film became sharp and the intensities of peaks increased considerably, which we ascribed to significant grain growth and densification of the Cu film.[24] No additional peaks were observed for higher-temperature annealing conditions until 800 °C, at which point peaks were detected of Cu_3Si(320), Cu_3Si(312) and Cu_4Si(440). That is to say, the small-grain SLG apparently served as a Cu diffusion barrier up to 800 °C. With annealing to 850 °C, the intensity of the Cu_3Si diffraction peaks was increased slightly, while the Cu_4Si diffraction peak was not observed and the Cu diffraction peaks were noticeably weakened due to the loss of metallic Cu by diffusion through the small-grain SLG barrier into Si. The absence of the Cu_4Si diffraction peak indicates that Cu_3Si is more stable than Cu_4Si at high temperatures.[25] XRD ω-2θ scans of Cu/large-grain SLG/Si samples before and after 30 min of annealing at different temperatures ranging from 500 to 900 °C are shown in Figure 2c. Contrastingly with the results of the small-grain SLG barrier, no copper silicide phases were observed after annealing at 800 and 850 °C. Even after annealing a Cu/large-grain SLG/Si sample at 900 °C, copper silicide phases did not form; however, both the Cu(111) and Cu(200) diffraction peaks decreased significantly due to evaporation of Cu at temperatures near its melting point (~1085 °C). The difference in thermal stability between the small- and large-grain SLG will be further discussed below.

To investigate barrier performance with respect to the thickness of the graphene layers, the barrier performance of MLG grown on Ni film was investigated using the same preparation method described for small- and large-grain SLG. XRD spectra of the Cu/MLG/Si samples before and after annealing in the temperature range of 500–900 °C for 30 min in an Ar and H_2 atmosphere are shown in Figure 2d. Similar to the small- and large-grain SLG barrier, the as-prepared samples containing an MLG barrier exhibited minor Cu (111) and Cu (200) peaks at 43.36° and 50.52°, respectively, and the intensities of theses peaks increased significantly with increasing annealing temperature, indicating Cu grain growth. A weak graphite (400) peak was observed at ~54.67° in the Cu/MLG/Si samples, indicating the transfer of multi-layer graphene to the Si substrate. Similar to what we observed for the large-grain SLG barrier, copper silicides did not form even after annealing at 900 °C. The results of XRD spectra for large-grain SLG and MLG illustrated that both large-grain SLG and MLG served as effective Cu diffusion barriers by preventing diffusion and remaining chemically inert even at temperatures as high as 900 °C. The fabricated large-grain SLG (~0.35 nm, one atom thick) exhibited the highest thermal stability reported so far for a diffusion barrier less than 2 nm thick. Even though the small-grain SLG barrier was less thermally stable than large-grain SLG barrier, it was still superior to other diffusion barrier materials with thicker thickness. Additionally, MLG (~10 nm, ~28 layers) also showed better thermal stability than other diffusion barrier materials with similar thicknesses. These results imply that graphene is an excellent diffusion barrier material candidate for ultra-large scale integrated technologies.

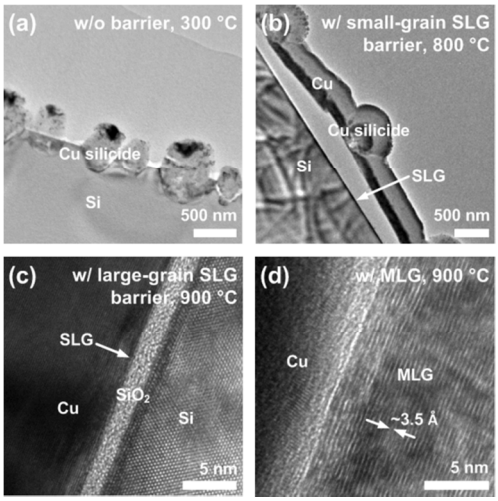

Figure 3. (a–b) Low-resolution TEM micrographs showing interactions at the Cu/Si interface, with and without graphene barriers: (a) sample with no diffusion barrier, after annealing at 400 °C and (b) sample with a small-grain SLG barrier, after annealing at 800 °C. (c-d) High-resolution TEM micrograph with graphene barriers, after annealing at 900 °C: (c) sample with a large-grain SLG barrier and (d) sample with MLG barrier.

To better understand the interface between the Cu film and the graphene layers, we examined cross-sectional TEM micrographs of Cu/small-grain SLG/Si, Cu/large-grain SLG/Si, and Cu/MLG/Si samples. Figure 3 shows typical TEM images of Cu/Si, Cu/small-grain SLG/Si, Cu/large-grain SLG/Si, and Cu/MLG/Si samples annealed for 30 min in an Ar and H_2 atmosphere. A representative cross-sectional TEM micrograph of a Cu/Si sample that was annealed at 300 °C is shown in Figure 3a. In the absence of a diffusion barrier, a huge elliptical copper silicide formed that was 300 nm long and 400 nm thick; the copper silicide grew deeply into the Si substrate, creating a gap between the copper silicide and the Si (Figure 3a). It has been determined previously that Cu is the dominant diffusion species in the formation of copper silicide.[26] Consistent with the XRD results shown in Figure 2b, a cross-sectional TEM micrograph of a Cu/small-grain SLG/Si stacked structure annealed at 800 °C shows that copper silicides were formed; a huge gap between the Cu film and the Si was also observed, caused by strains and stresses produced due to lattice mismatch between the Si and the formed copper silicide (Figure 3b). A high-resolution TEM image of the interfacial region of the Cu/large-grain SLG/Si stacked structure annealed at 900 °C is shown in Figure 3c; even though the large-grain SLG layer could barely be distinguished (see arrow in Figure 3c), no interdiffusion between Cu and Si was observed, the Cu film remained adhered to the layer below, and the interface was clean. We observed a 2-nm-thick native oxide layer on Si in Figure 3c. The silicon native oxide layer would be inevitably formed during the graphene transfer process even though we immersed the Si substrate in diluted hydrofluoric acid (HF) aqueous solution for 1 min before the graphene transfer. As we already confirmed in Figure 2a that Cu_3Si phases were formed after annealing the as-prepared Cu/Si sample at 300 °C, which has native oxide layer on Si, the silicon native oxide layer cannot block the Cu diffusion into Si.[27]

The lattice spacing of the Ni-grown MLG was determined to be approximately 0.35 nm by high- resolution TEM (HR-TEM) analysis of the Cu/MLG/Si structure, confirming the presence of a two-dimensional carbon structure (Figure 3d); the thickness of the MLG ranged from 5 to 10 nm, which corresponds to 14–28 layers of graphene. An adhesively layered Cu and MLG structure was observed, with a clear interface between the Cu film and MLG layers and no sign of compound formation. Moreover, there was no evidence of intermixing between Cu and Si based on the HR-TEM images.

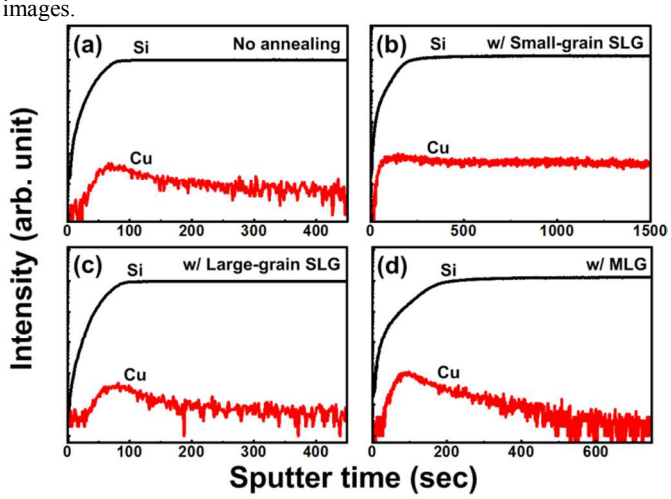

Figure 4. The ToF-SIMS SIMS depth profile of Cu diffused into the Si substrate of the (a) large-grain SLG/Si sample before annealing (a reference sample), (b) small-grain SLG/Si sample after annealing at 900 °C, (c) large-grain SLG/Si sample after annealing at 900 °C, and (d) MLG/Si sample after annealing at 900 °C.

The time-of-flight secondary ion mass spectroscopy (ToF-SIMS) depth profile measurement was performed to precisely examine if even an extremely small quantity of Cu can penetrate into the Si substrate through the graphene barrier. For our ToF-SIMS measurement, we prepared three types of samples: Cu/small-grain SLG/Si, Cu/large-grain SLG/Si, and Cu/MLG/Si. These samples were then annealed at 900 °C under the same conditions used in the XRD analysis. We used another Cu/large-grain SLG/Si sample as a reference sample, which was not annealed. Prior to the ToF-SIMS depth profile analysis, Cu layers on graphene barriers of each samples were removed by soaking the samples in diluted nitric acid (30 %) for 15 min. Figure 4 shows the ToF-SIMS depth profiles of Si and Cu atom obtained from the Si substrate of each samples. In case of the non-annealed Cu-etched/large-grain SLG/Si reference sample (Figure 4a), the Si substrate region is clearly distinguished by the rapid increase and saturation of the Si signal, while in case of Cu intensity, it decreases gradually with sputtering time. Negligible surface Cu intensity was due to the knock-on effect of the remaining Cu atoms on the top of the sample surface.[28] The depth profile result of reference sample allows the elimination of possible artificial errors in the ToF-SIMS analysis. As shown in Figure 4b, for the Cu-etched/small-grain SLG/Si sample, the ToF-SIMS depth profile clearly shows the Cu penetration into the Si substrate; the Cu signal rapidly increased and saturated. In contrast, the ToF-SIMS depth profiles of both Cu-etched/large-grain SLG/Si and Cu-etched/MLG/Si samples have an almost similar Cu distribution and intensity throughout the sputtering time as that of the reference sample (Figure 4c and d), which indicates no detectable Cu penetration into the Si substrate through the large-grain SLG and MLG barriers. These results agree well with the XRD and TEM results which indicate the large-grain SLG and the MLG have significantly higher thermal stability than other materials.

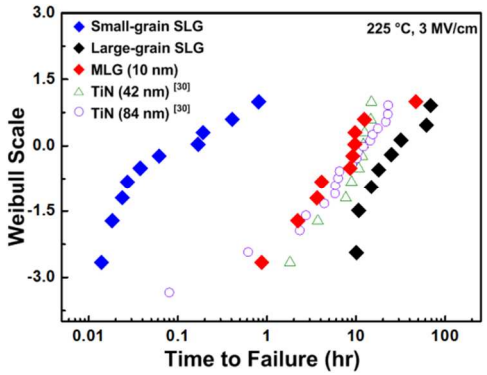

Figure 5. Weibull plots of time to failure for small-grain SLG, large-grain SLG, MLG, and TiN diffusion barriers.

Even though we confirmed that small-grain SLG, large-grain SLG, and MLG work well as Cu diffusion barriers at temperatures as high as 700 and 900 °C, diffusion barrier characteristics should also be evaluated under real device operation conditions, because Cu interconnect in actual devices is affected by electric fields as well as thermal stresses. Under real device operating conditions, positive Cu ions can drift into the dielectric layer under an electric field.[29] To evaluate the ability of graphene to function as a Cu diffusion barrier under device operating conditions, we performed TDDB tests by monitoring the leakage current of the dielectric layer, and compared the results to TDDB data collected by Lee *et al.* on Cu diffusion barriers of 42- and 84-nm-thick TiN.[30] Both herein and in the work of Lee *et al.,* the failure criterion used was a leakage current of 1×10^{-5} A; all tests were carried out under the same conditions of electric field (3 MV/cm) and temperature (225 °C). Weibull plots of TDDB time to failure (TTF) are shown in Figure 5; the characteristic times ($t_{63.2}$) were 0.15, 34.14, 10.91, 11.81, and 14.20 h for MIS samples with barrier layers of small-grain SLG, large-grain SLG, MLG, 42-nm-thick TiN, and 84-nm-thick TiN, respectively. Even though the large-grain SLG was only one atom thick, one of the thinnest barrier layers that we examined, it had the longest TTF of more than 10 h. On the other hand, small-grain SLG had the shortest TTF of less than 1 h. The MLG had a shorter TTF than the large-grain SLG, despite the latter's relative thinness; somewhat similarly, the MLG and TiN barriers had similar TTFs despite the former's relative thinness. These results indicate that the near-zero-thickness large-grain SLG diffusion barrier has outstanding barrier performance under an electric field, as well as in response to thermal stress. The barrier performance of MLG was superior to that of TiN, but inferior to that of large-grain SLG.

Contrary to our expectation that MLG would have the longest TTF among the graphene barrier samples, it was large-grain SLG that actually had the longest TTF, though MLG indeed outperformed small-grain SLG in this respect. Possible reasons for this trend are the effects of both the graphene thickness and the grain size of the CVD-grown polycrystalline SLG and MLG. As discussed above, SLG grown on Cu foil was dominated by basal planes, whereas MLG grown on Ni film was dominated by edge planes (recall Figure 1a). The movement of metal atoms or metal ions likely occurred along the edge planes of MLG; in other words, the edge planes of MLG likely acted as reactive diffusion sites for Cu atoms and ions. Yao *et al*. recently investigated Li ion diffusion through SLG and MLG and concluded that Li ions diffused well along edge planes, while pure basal planes of graphene allowed only lateral diffusion of Li ions.[31] This explains why the thick MLG grown on Ni film was an inferior diffusion barrier relative to the thin, large-grain SLG in our experiments. Then, grain size could be the main factor that determines the diffusion barrier performance of graphene barriers. Despite the fact that the grain boundaries of polycrystalline CVD-grown graphene continuously connect each grain with strong bonding, they nonetheless constitute the weakest region of the material and can eventually act as diffusion pathways for Cu atoms or ions. In fact, grain boundary dislocation of graphene is likely to weaken its overall mechanical strength; this has been confirmed by tearing tests in previous studies.[32] Topsakal et al. also showed that the grain boundaries of graphene can operate as diffusion pathways for oxygen transport based on a theoretical analysis.[33]

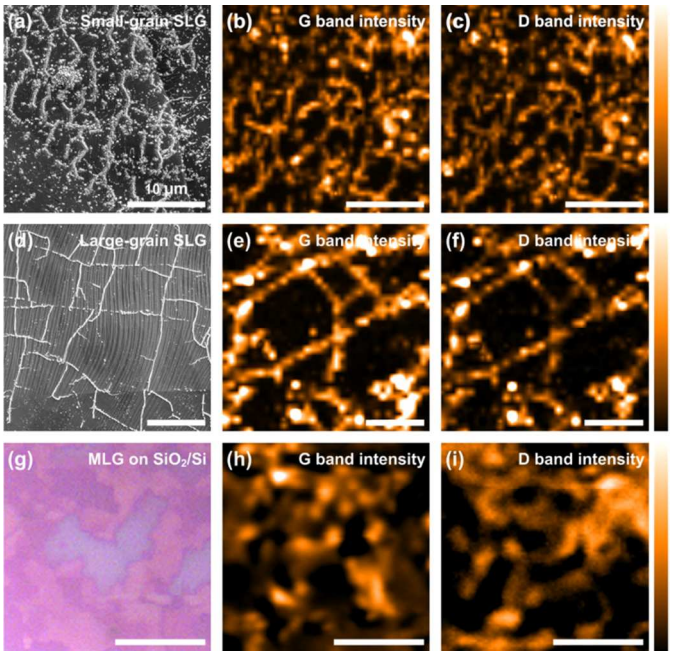

Figure 6. Micrographs and integrated intensity Raman maps of (a–c) small-grain SLG/Cu, (d–f) large-grain SLG/Cu, and (g–i) MLG transferred onto a SiO_2/Si substrate: (a, d) FE-SEM micrographs of SLG/Cu samples after selective oxidation at 200 °C in air for 4 h; (g) optical micrograph of MLG; (b, e, h) integrated intensity Raman maps of the graphene G band (1560–1610 cm^{-1}); (c, f, i) integrated intensity Raman maps of the graphene D band (1350–1390 cm^{-1}). All scale bars indicate 10 μm.

The detailed grain sizes of our SLG barriers were examined with optical microscope images, FE-SEM images and a confocal Raman mapping of the G band (1560–1610 cm^{-1}) and D band (1350–1390 cm^{-1}) with a 633 nm excitation laser after selective oxidation of Cu foil below SLG using a previously reported method.[34] The selective oxidation process was realized by selectively oxidizing the Cu foil through SLG grain boundaries under moisture-rich ambient conditions. The formation of Cu_2O on Cu foil through SLG grain boundaries allows us to probe SLG grain boundary lines with an optical microscope. The grain size of the MLG barrier was confirmed by performing a confocal Raman mapping of the G band (1560–1610 cm^{-1}) and D band (1350–1390 cm^{-1}) with a 532 nm excitation laser with a transferred MLG sample onto 300-nm-thick SiO_2/Si substrate. FE-SEM images and corresponding Raman maps that provide information on graphene thickness, graphene grain boundaries, and defect densities are presented in Figure 6. The formation of Cu_2O through SLG grain boundaries under moisture-rich ambient conditions was evident in both the small- and large-grain SLG samples by white dotted lines appearing in FE-SEM images;[34] the grain size of the small-grain SLG ranged from 1 to 3 μm, while the grain size of the large-grain SLG ranged from 6 to 12 μm (Figure 6a and d). To confirm the

evidence for Cu_2O formation along the grain boundaries of graphene layer after selective oxidation in air we performed energy-dispersion spectrometry (EDS) point measurements and Raman spectrum measurements on a large-grain SLG/Cu foil sample. The EDS analysis showed sharp peaks of Cu and O along the grain boundary region, further confirming the presence of Cu oxide (Figure S1). The Raman analysis showed the well-established broad Raman bands attributable to Cu_2O at 526 and 603 cm^{-1}, confirming the type of Cu oxide species.[35] Even though both small- and large-grain SLG samples were annealed under the same conditions, the density of oxidized states was higher in small-grain SLG than in large-grain SLG because the former has higher density of grain boundary states. This trend in grain boundary density was confirmed using confocal Raman mapping of the G and D bands; the mapping in the D and G band matched well with the grain boundaries observed in SEM images (Figure 6b-c, 6e-f). An optical image and Raman G and D band maps of the MLG are presented in Figure 6g-i. The optical image of the MLG shows the presence of multilayer graphene that formed on the Ni film by the precipitation of carbon species (Figure 6g). In the G band map of Figure 6h, the thinnest regions of the MLG are shown as dark areas, while the thickest regions of MLG are shown as bright areas. Compared to small- and large-grain SLG, the MLG showed a greater variation in G band intensity, indicating the formation of non-uniform, multilayered flakes. Despite the discontinuity of the MLG's top surface, single- and few-layer graphene bridged together to create a continuous film over the entire film area. The MLG also had a greater variation in D band intensity, indicating that grains of many different thicknesses were present, with many defects caused by the numerous edge planes (Figure 6i) Because of this variation in flake thickness, we could not accurately determine the grain size of the MLG; nonetheless, its grain size could be estimated as less than 6 μm, assuming based on the areas of the less defective regions in the D band map (dark areas in Figure 6i). Comparing grain size between large-grain SLG and MLG clearly showed that large-grain SLG grown on Cu had larger grains than MLG grown on Ni. Contrastingly, the grain size of the small-grain SLG was smaller than that of the MLG. These results confirm that the diffusion barrier performance of graphene can be improved by increasing the size of its grains because Cu atoms or ions diffuse through grain boundaries.

3. Experimental section

Sample preparation: For the growth of SLG, 25-μm-thick annealed Cu foil (99.8 % metals basis, Alfa Aesar 13382) was cut into 1 × 1 cm^2 pieces that were successively cleaned by ultrasonication in acetone, isopropyl alcohol, and de-ionized (DI) water for 10 min each. The prepared samples were loaded into a CVD quartz chamber and SLG was synthesized on their surfaces as described elsewhere.[36] To fabricate large-grain SLG, Cu foil samples were first annealed by heating them to 1077 °C under hydrogen gas flow (H_2, 50 sccm) for 60 min at atmospheric pressure, and then the graphene was formed by adjusting the chamber pressure to 2 Torr under a continuous flow of H_2 and CH_4 (10 sccm) as carrier gases at 1000 °C for 60 min. The fabrication of small-grain SLG was carried out by heating Cu foil samples to 1000 °C under hydrogen gas flow (H_2, 50 sccm) for 20 min, followed by annealing for 60 min under a continuous flow of H_2 and CH_4 carrier gases (10 sccm) at 1000 °C. For the growth of MLG, 500-nm-thick Ni films were thermally evaporated onto 1 × 1 cm^2 SiO_2/Si substrates and cleaned by the ultrasonication process described above; prepared Ni/SiO_2/Si samples were then annealed at 1000 °C under H_2 flow (500 sccm) for 20 min, followed by further annealing at 1000 °C for 5 min with the introduction of CH_4 (50 sccm). Selective oxidation of Cu foil below the SLG was carried out on a hot plate at 200 °C in air for 4 h. The ambient temperature was 24.5 °C and the relative humidity was 53□63%.

To transfer the SLG/Cu and MLG/Ni/SiO_2/Si samples, poly(methyl methacrylate)(PMMA) solution (PMMA powder from Sigma Aldrich; average molar weight ~996,000, product no. 182265, dissolved in anisole to a concentration of 40 mg/ml) was spin-coated at 4200 rpm for 40 s and dried at room temperature in a vacuum chamber for 30 min. The Cu foil was etched in a 0.1M ammonium persulfate solution and Ni was etched in a 1:5:4 aqueous solution of hydrofluoric acid (HF), nitric acid (HNO_3), and H_2O. The resulting PMMA/graphene structures floated on the etching solution; using a glass substrate, they were moved to a 5:1:1 solution of H_2O/H_2O_2/HCl and kept there for 15 min to remove etchant residue. The PMMA/graphene stacked structures were rinsed with DI water several times for 10 min each using the same procedure. The cleaned PMMA/graphene structures were manually laid on cleaned p-type (100) Si substrates. The Si substrate was cleaned by dipping in a dilute HF solution (HF:H_2O = 1:50) for 1 min to remove native oxides before the graphene transfer.

To remove the PMMA supporting layer, the PMMA/graphene on the Si substrate was immersed in an acetone solution for 10 min and then annealed in a furnace at 400 °C for 3 h while flowing a 1:1 mixture of Ar and H_2 gases. Then, 500-nm-thick Cu film was deposited on the graphene/Si substrates via a vacuum thermal evaporating system using a shadow mask with square patterns approximately 1.5 mm on a side. Finally, to analyze the thermal stability of graphene as a diffusion barrier, the prepared samples were annealed at temperatures ranging from 500 to 900 °C for 30 min each in a mixture of Ar and H_2 gases.

To prepare the TDDB test samples, SLG and MLG samples were transferred onto (100) oriented n-type Si substrate (0.001 – 0.003 Ω · cm) covered with a 100-nm-thick thermally grown SiO_2 layer. Then, 300-nm-thick Cu film was deposited on graphene/SiO_2/n-type Si substrates using a vacuum thermal evaporating system and a shadow mask with a circular pattern 600 μm in diameter. To avoid oxidation of Cu during the test, an Al/Ta (500 nm/50 nm) bilayer was deposited by DC magnetron sputtering through the same shadow mask used to evaporate the Cu films. To fabricate the backside electrode, a 500-nm-thick Al layer was deposited on the back side of the Si substrate via DC magnetron sputtering after removing the native oxide with 5% HF aqueous solution. TDDB tests were performed at 225 °C and 3 MV/cm using a low leakage multimeter (Kiethley ^{TM} 237).

Characterization: Samples of SLG and MLG synthesized on a SiO_2/Si substrate were observed using an optical microscope equipped with a mounted digital camera (Artcam 300MI). Raman spectroscopy and spatial Raman mapping were performed using a micro-Raman system (Jobin-Yvon, LabRam HR) equipped with a motorized sample stage. The wavelengths of the excitation laser were 532 and 633 nm, its power was set to 5mW, and its spot size was approximately 1 μm. The pixel of the Raman maps was 300 nm square. Transition of Cu into the copper silicide phase was analysed using an XRD system (Rigaku, D/Max-2500H) with a Cu $K_{\alpha 1}$ source (λ = 1.540562 Å), operated at 40 kV and 100 mA. A FE-SEM (JEOL, 7001F) was used to examine the surface morphology of graphene/Cu samples. The ToF-SIMS depth profiling was performed on an Ion TOF (Munster, Ion-TOF IV) equipped with both Bi^{3+} and Cs^+ primary ion beam sources. The analysis source was a pulsed 3 kV Bi^{3+} beam, and the target current was ~ 1.4 pA with an acquisition area of 100 × 100 μm^2. The sputter ion source was a 1 kV Cs^+ primary ion beam, which bombarded the surface at an incident angle of 45° to the normal surface. The

target current was maintained at ~ 20 nA and the sputtering area was 400 × 400 μm^2. The elemental composition of Cu_2O on Cu after selective oxidation was investigated with the SEM-EDS link system (JEOL, 3000F). A TEM (JEOL, 3000F) equipped with an energy dispersive spectroscopy measurement system was used to identify phases and to study interfacial reactions of cross-sectional material samples. The root mean square roughness of graphene transferred onto the SiO_2/Si substrate was investigated using AFM (Park system Co., XE-100).

Conclusions

We demonstrated the ability of single-layer and multi-layer graphene to act as Cu diffusion barriers by performing diffusion tests in different temperature regimes (500–900 °C) for 30 min while flowing a mixture of Ar and H_2 gases. Results from the XRD, TEM, and ToF-SIMS analyses confirmed that SLG and MLG effectively blocked the diffusion of Cu atoms into Si. The intrinsic barrier performance of Cu/graphene barrier/SiO_2 structures were also investigated by TDDB tests performed at 225 °C under positive bias (3 MV/cm) to determine whether graphene could act as a Cu diffusion barrier under real device operating conditions. SLG of 10 μm average grain size exhibited excellent TDDB performance compared to TiN and MLG. To the best of our knowledge, the Cu diffusion barrier performance reported herein for SLG less than 2 nm thick is the best reported thus far; in other words, graphene is an effective near-zero-thickness Cu diffusion barrier. To further improve the barrier performance of the SLG diffusion barrier, it is necessary to ensure high-quality growth with large grain size, because the grain boundaries are vulnerable to diffusion of Cu atoms.

Acknowledgements

This work was supported by the National Research Foundation of Korea(NRF) grant funded by the Korea government(MEST) (No. 2011-0028594). This work was supported by the Priority Research Centers Program through the National Research Foundation of Korea (NRF) funded by the Ministry of Education, Science and Technology (2012-0006689).

Notes and references

[a] Nanobio Device Laboratory, School of Electrical and Electronic Engineering, Yonsei University, 50 Yonsei-ro, Seodaemun-Gu, Seoul, 120-749, Republic of Korea; E-mail: taeyoon.lee@yonsei.ac.kr

[b] Nanodevice Materials Laboratory, Department of Materials Science & Engineering, Seoul National University, 1 Gwanak-ro, Gwanak-Gu, Seoul 151-744, Republic of Korea

[c] in-situ Electron Microscopy Laboratory, Department of Materials Science and Engineering, Seoul National University, 599 Gwanak-ro, Gwanak-Gu, Seoul, 31-411, Republic of Korea

[d] Nanodevice Laboratory, School of Electrical and Electronic Engineering, Yonsei University, 50 Yonsei-ro, Seodaemun-Gu, Seoul 120-749, Republic of Korea

[e] Microwave Integrated Circuits and Systems Laboratory, School of Electrical and Electronic Engineering, Yonsei University, 50 Yonsei-ro, Seodaemun-Gu, Seoul 120-749, Republic of Korea

Electronic Supplementary Information (ESI) available: [details of any supplementary information available should be included here]. See DOI: 10.1039/c000000x/

1. a) S. Tsukimoto, T. Morita, M. Moriyama, K. Ito, M. Murakami, *J. Electron. Mater.* 2005, **34,** 592; b) C. H. Lin, W. K. Leau, *J. Electron. Mater*. 2009, **38,** 2212; c) G. Schneiderm, D. Hamback, B. Niemann, B. Kaulich, J. Susini, N. Hoffmann, W. Hasse, *Appl. Phys. Lett*. 2001, **78**, 1936.
2. a) C. Chang, *J. Appl. Phys.* 1990, **67**, 566; b) T. Nitta, T. Ohmi, M. Otsuki, T. Takewaki, T. Shibata, *J. Electrochem. Soc.* 1992, **139**, 922.
3. a) M. T. Wang, Y. C. Lin, M. C. Chen, *J. Electrochem. Soc.* 1998, **145**, 2538; b) Q. Xie, X. P. Qu, J. J. Tan, Y. L. Jiang, M. Zhou, T. Chen, G. P. Ru, *Appl. Surf. Sci*. 2006, **253**, 1666.
4. *The International Technology Roadmap for Semiconductors*, Available from www.itrs.net, 2012.
5. D. Josell, S. H. Brongersma, Z. Tokei, *Annu. Rev. Mater. Res.* 2009, **39**, 231.
6. a) K. C. Hsu, D. C. Perng, J. B. Yeh, Y. C. Wang, Appl. Surf. Sci. 2012, **258**, 7225; b) S. F. Ding, Q. Xie, F. Chen, H. S. Lu, S. R. Deng, D. Deduytsche, C. Detavernier, X. P. Qu, ECS Solid State Lett. 2012, **1**, 54; c) W. Wu, S. H. Brongersma, M. V. Hove, K. Maex, Appl. Phys. Lett. 2004, **84**, 2838; d) A. E. Kaloyeros, E. T. Eisenbraunm K. Dunn, O. van der Straten, Chem. Eng. Comm. 2011, **198**, 1453.
7. M. A. Khaderbad, R. Pandharipande, V. Singh, S. Madhu, M. Ravikanth, V. R. Rao, IEEE T. Electron Dev. 2012, **59**, 1963.
8. J. Koike, M. Wada, Appl. Phy. Lett. 2005, **87**, 041911.
9. K. C. Hsu, D. C. Perng, Y. C. Wang, J. Alloy. Compd. 2012, **516**, 102.
10. a) A. K. Geim, K. S. Novoselov, Nat. Mater. 2007, **6**, 183; b) J. S. Bunch, A. M. van der Zande, S. S. Verbridge, I. W. Frack, D. M. Tanenbaum, J. M. Parpia, H. G. Craighead, P. L. McEuen, Science 2007, **315**, 490; c) J. C. Meyer, A. K. Geim, M. I. Katsnelson, K. S. Novoselov, T. J. Booth, S. Roth, Nature 2007, **446**, 60.
11. a) T. Georgiou, L. Britnell, P. Blake, R. V. Gorbachev, A. Gholinia, A. K. Geim, C. Casiraghi, K. S. Novoselov, Appl. Phys. Lett. 2011, **99**, 093103; b) O. Leenaerts, B. Partoens, F. M. Peeters, Appl. Phys. Lett. 2008, **93**, 193107; c) J. S. Bunch, S. S. Verbridge, J. S. Alden, A. M. van der Zande, J. M. Parpia, H. G. Craighead, P. L. McEuen, Nano Lett. 2008, **8**, 2458; d) S. Chen, L. Brown, M. Levendorf, W. Cai, S. Y. Ju, J. Edgeworth, X. Li, C. W. Magnuson, A. Velamakanni, R. D. Piner, J. Kang, J. Park, R. S. Ruoff, ACS Nano 2011, **5**, 1321.
12. H. Y. Kim, C. Lee, J. Kim, F. Ren, S. J. Pearton, J. Vac. Sci. Technol. B 2012, **30**, 030602-1.
13. C. G. Kang, S. K. Lim, S. Lee, S. K. Lee, C. Cho, Y. G. Lee, H. J. Hwang, Y. Kim, H. J. Choi, S. H. Choe, M. H. Ham, B. H. Lee, Nanotechnology 2013, **24**, 115707.
14. a) C. H. Yeh, H. Medina, C. C. Lu, K. P. Huang, Z. Liu, K. Suenage, P. W. Chiu, ACS Nano 2014, **8**, 275; b) Y. Xue, B. Wu, L. Jiang, Y. Guo, L. Huang, J. Chen, J. Tan, D. Geng, B. Luo, W. Hu, G. Yu, Y. Liu, J. Am. Chem. Soc. 2012, **134**, 11060; c) J. Kwak, J. H. Chu, J. K. Choi, S. D. Park, H. Go, S. Y. Kim, K. Park, S. D. Kim, Y. W. Kim, E. Yoon, S. Kodambaka, S. Y. Kwon, Nat. Comm. 2012, **3**, 645; d) B. Dlubak, M. B. Martin, R. S. Weatherup, H. Yang, C. Deranlot, R. Blume, R. Schloegl, A. Fert, A. Anane, S. Hofmann, P. Seneor, J. Robertson, ACS Nano 2012, **6**, 10930.
15. S. J. Chae, F. Gune, K. K. Kim, E. S. Kim, G. H. Han, S. M. Kim, H. J. Shin, S. M. Yoon, J. Y. Choi, M. H. Park, C. W. Yang, D. Pribat, Y. H. Lee, Adv. Mat. 2009, **21**, 2328.
16. D. Graf, F. Molitor, K. Ensslin, C. Stampfer, A. Jungen, C. Hierold, L. Wirtz, Nano Lett. 2007, **7**, 238.
17. S. Ryu, L. Liu, S. Berciaud, Y. J. Yu, H. Liu, P. Kim, G. W. Flynn, L. E. Brus, Nano. Lett. 2010, **10**, 4944.
18. A. C. Ferrari, J. C. Meyer, V. Scardaci, C. Casiraghi, M. Lazzeri, F. Mauri, S. Piscanec, D. Jiang, K. S. Novoselov, S. Roth, A. K. Geim, Phys. Rev. Lett. 2006, **97**, 187401.

19. Q. Yu, J. Lian, S. Siriponglert, H. Li, Y. P. Chen, S. S. Pei, Appl. Phys. Lett. 2008, **93**, 113103.
20. J. C. Zhou, Y. Z. Li, D. H. Huang, J. Mater. Process. Technol. 2009, **209**, 774.
21. a) P. Majumder, C. G. Takoudis, Appl. Phys. Lett. 2007, **91**, 162108; b) S. S. Song, Y. Z. Liu, D. L. Miao, H. Q. Ling, M. Li, Thin solid films, 2005, **476**, 142; c) C. A. Chang, J. Appl. Phys. 1989, **68**, 1163; d) L. Wang, Z. H. Cao, K. Hu, Q. W. She, X. K. Meng, Mater. Chem. Phys. 2012, **135**, 806.
22. a) T. Oku, E. Kawakami, M. Uekubo, K. Takahiro, S. Yamaguchi, M. Murakami, Appl. Surf. Sci. 1996, **99**, 265; b) L. Stolt, A. Charai, F. M. D'Heurle, P. M. Fryer, J. M. E. Harper, J. Vac. Sci. Tec. A. 1991, **9**, 1501.
23. a) L. C. Leu, D. P. Norton, L. McElwee-White, T. J. Adnerson, Appl. Phys. Lett. 2008, **92**, 111917; b) Y. Wang, C. C. Zhu, Z. Song, Y. Li, Microelectron. Eng. 2004, **71**, 69.
24. a) C. M. Liu, W. L. Liu, W. J. Chen, S. H. Hsieh, T. K. Tsai, L. C. Yang, Electrochem. Soc. 2005, **152**, G234; b) S. H. Kim, K. T. Nam, A. Datta, H. M. Kim, K. B. Kim, D. H. Kang, J. Vac. Sci. Tec. B. 2003, **21**, 804.
25. N. Benouattas, A. Mosser, D. Raiser, J. Faerber, A. Bouabellou, Appl. Surf. Sci. 2000, **153**, 79.
26. a) L. Stolt, F. M. D'Heurle, J. M. E. Harper, Thin Solid Films 1991, **200**, 147; b) C. S. Lee, H. Gong, R. Liu, A. T. S. Wee, C. L. Cha, A. See, L. Chan, J. Appl. Phys. 2001, **90**, 3822.
27. A. M. Caro, S. Armini, O. Richard, G. Maes, G. Borghs, C. M. Whelan, Y. Travaly, Adv. Funct. Mater. 2010, **20**, 1125.
28. R. Chan, T. N. Arunagiri, Y. Zhang, O. Chyan, R. M. Wallace, M. J. Kim, T. Q. Hurd, Electrochem. Solid State Lett. 2004, **6**, G154.
29. a) H. W. Yeon, S. Y. Jung, J. R. Lim, J. Pyun, H. Kim, D. Back, Y. C. Joo, Electrochem. Solid State Lett. 2012, **15**, H157; b) S. Y. Jung, B. J. Kim, N. Y. Lee, B. M. Kim, S. J. Yeom, N. J. Kwak, Y. C. Joo, Microelectron. Eng. 2012, **89**, 58.
30. Y. J. Lee, H. W. Yeon, S. Y. Jeong, S. K. Na, J. S. Park, Y. Y. Choi, O. S. Song, Y. C. Joo, Electron. Mater. Lett., DOI: 10.1007/s13391-013-3108-0
31. F. Yao, F. Gunes, H. Q. Ta, S. M. Lee, S. J. Chae, K. Y. Sheem, C. S. Cojocaru, S. S. Xie, Y. H. Lee, J. Am. Chem. Soc. 2012, **134**, 8646.
32. a) J. Kotakoski, J. C. Meyer, Phy. Rev. B. 2012, **85**, 195447; b) A. Cao, Y. Yuan, Appl. Phys. Lett. 2012, **100**, 211912.
33. M. Topaskal, H. Sahin, S. Ciraci, Phys. Rev. B 2012, **85**, 155445.
34. a) D. L. Duong, G. H. Han, S. M. Lee, F. Gunes, F. S. Kim, S. T. Kim, H. Kim, Q. H. Ta, K. P. So, S. J. Yoon, S. J. Chae, Y. W. Jo, M. H. Park, S. H. Chae, S. C. Lim, J. Y. Choi, Y. H. Lee, Nature 2012, **490**, 235; b) S. S. Roy, M. S. Arnold, Adv. Funct. Mater. 2013, **23**, 3638.
35. a) H. Y. H. Chan, C. G. Takoudis, M. H. Weaver, J. Phys. Chem. B. 1999, **103**, 357; b) F. Texier, L. Servant, J. L. Bruneel, F. Argoul, J. Electroanal. Chem. 1998, **446**, 189.
36. a) H. Wang, G. Wang, P. Bao, S. Yang, W. Zhu, X. Xie, W. J. Zhang, J Am. Chem. Soc. 2012, **134**, 3627; b) S. H. Lee, K. H. Lee, Z. Zhong, Nano Lett. 2010, **10**, 4702.

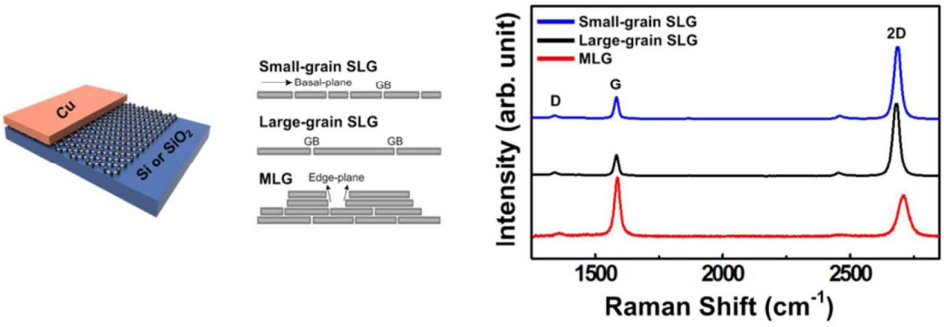

We investigate the ability of both single-layer and multilayer graphene grown by chemical vapor deposition (CVD) to act as Cu diffusion barriers.